Available online at www.sciencedirect.com
ScienceDirect
Polymer 48 (2007) 6923–6933
polymer
www.elsevier.com/locate/polymer

An improved technique for exfoliating and dispersing nanoclay particles into polymer matrices using supercritical carbon dioxide

Quang T. Nguyen, Donald G. Baird*

Department of Chemical Engineering, Virginia Polytechnic Institute and State University, Blacksburg, VA 24061-0211, United States

Received 18 May 2007; received in revised form 3 September 2007; accepted 4 September 2007
Available online 14 September 2007

Abstract

An environmentally benign process, which uses supercritical carbon dioxide (sc-CO_2) as a processing aid, is developed in this work to help exfoliate and disperse nanoclay into the polymer matrices. The process relies on rapid expansion of the clay followed by direct injection into the extruder where the mixture is dispersed into the polymer melt. Results from the mechanical properties, rheological studies, and X-ray diffraction (XRD) show that this method represents a significant improvement relative to direct melt blending in single or twin-screw extruders or other methods using sc-CO_2. The greatest mechanical property response was a result of directly injecting pre-mixed sc-CO_2 and nanoclay into the polypropylene melt during extrusion. It was observed that for concentrations as high as 6.6 wt% (limited only by present process capabilities), XRD peaks were eliminated, suggesting a high degree of exfoliation. Mechanical properties such as modulus increased by as much as 54%. The terminal region of the dynamic mechanical spectrum was similar to that of the base polymer, contrary to what is frequently reported in the literature.

Keywords: Nanocomposites; Nanoclay; Supercritical carbon dioxide

1. Introduction

1.1. Polymer–clay nanocomposites

During the last decade, interest in polymer layered silicate nanocomposites has rapidly been increasing at an unprecedented level, both in industry and in academia, due to their potential for enhanced physical, chemical, and mechanical properties compared to conventionally filled composites [1–6]. They have the potential of being a low-cost alternative to high-performance composites for commercial applications in both the automotive and the packaging industries. It is well established that when layered silicates are uniformly dispersed and exfoliated into a polymer matrix, the polymer properties can be improved to a dramatic extent. These improvements may include increased strength [7], higher modulus [8–13], thermal stability [5,14,15], barrier properties [16,17], and decreased flammability [18–21]. Hence, in order to capitalize on the potential offered by nanoparticles in areas such as reinforcement, barrier, and electrical conductivity, higher levels of fully dispersed nanoparticles must be obtained.

Polymer–clay nanocomposites (PCNs) are two-phase materials in which the polymers are reinforced by nanoscale fillers. The most heavily used filler material is based on the smectite class of aluminum silicate clays, of which the most common representative is montmorillonite (MMT). MMT has been employed in many polymer–clay nanocomposite systems because it has a potentially high aspect ratio and high surface area that could potentially lead to materials with significantly improved properties. Additionally, it is environmentally friendly, naturally occurring, and readily available in large quantities.

Layered silicates in their pristine state are hydrophilic. Most of the engineering polymers are hydrophobic. Therefore,

* Corresponding author. Tel.: +1 540 231 5998; fax: +1 540 231 2732.
E-mail address: dbaird@vt.edu (D.G. Baird).

0032-3861/$ - see front matter © 2007 Elsevier Ltd. All rights reserved.
doi:10.1016/j.polymer.2007.09.015

dispersion of native clays in most polymers is not easily achieved due to the intrinsic incompatibility of hydrophilic layered silicates and hydrophobic engineering polymers [11]. In order to successfully develop clay-based nanocomposites, it is necessary to chemically modify a natural clay so that it can be compatible with a chosen polymer matrix. Generally, this can be done through ion exchange reactions by replacing interlayer cations with quaternary alkylammonium or alkylphosphonium cations [22–24].

One polymer of significant interest to industries such as the automotive sector is polypropylene (PP), but PP is one of the most non-polar polymers and has no polar groups in its backbone. Thus, interfacial bonding between the clay surface and the PP matrix is unfavorable. Recent attempts to increase the compatibility between the nanoclays and the PP matrix introduced two major methods including melt intercalation [25–30] and in situ polymerization [31]. The latter method usually involves a slurry phase, which requires large volumes of solvents and a need of purification. Thus this method may be impractical due to the high costs associated with the solvents, their disposal, and their impact on the environment. The method of melt intercalation does not require a solvent, but usually involves the use of a compatibilizer, such as maleic anhydride grafted PP (PP-*g*-MA), to facilitate the intercalation of PP in clay [25–27]. However, in spite of improved homogeneity and properties, complete exfoliation is practically never reached [28–42]. Usually a mix between intercalated and partially exfoliated structure is frequently observed. Also, in order to achieve a good level of intercalation at high clay concentration, a high ratio of PP-*g*-MA must be used. However, using a high level of PP-*g*-MA can be expensive and may reduce the nanocomposite's elongation at break and mechanical properties.

1.2. Supercritical carbon dioxide

To overcome some of the issues with using melt intercalation and modified PP and other solvent-based techniques, recently, there has been considerable interest in using sc-CO_2 as an alternative route for the preparation of polymer–clay nanocomposites [43–48]. A recent approach to prepare polymer nanocomposites using sc-CO_2 in the melt intercalation process was reported by Lesser et al. [44]. They used a modified hopper in the feed section of the extruder to allow polymer and clay to interact with sc-CO_2 before processing. It was found that the presence of sc-CO_2 promotes significant increase in the basal spacing of the clay, and thereby may enhance the ease of the polymer intercalation into the galleries of the clay. In a different approach, Mielewski et al. [47] proposed a method to directly inject sc-CO_2 into a melt mixture of silicate particles and polymer in an extruder. The silicates are expected to exfoliate when exiting the extruder. No WAXD or TEM evidence of exfoliated morphology was presented. Alternatively, Manke et al. [48] developed a process that allows clay particles to be pre-treated with sc-CO_2 in a pressurized vessel and then rapidly depressurized into another vessel at atmospheric pressure to force the clay platelets apart. The result was exfoliated nanoclay particles as observed by X-ray diffraction. However, they did not provide any mechanism for assuring that the exfoliated particles remain exfoliated when they are combined with the polymer via conventional melt blending.

In this study, we develop a process to help exfoliate and disperse the nanoclay into PP matrix with the aid of supercritical CO_2. The process involves the use of a pressurized CO_2 chamber to assist in the exfoliation and delivery of the clay into a stream of polymer melt in the extruder. This process is different from the systems previously mentioned above in a way that it allows only the clay to be in direct contact with sc-CO_2, as opposed to both clay and polymer as described in Lesser's and Mielewski's processes, and that the mixture of exfoliated clay and sc-CO_2 is fed into the extruder in a one-step process instead of a two-step like Manke's process. This CO_2 method is evaluated and compared to other processing methods including the direct melt-blending technique using a single-screw extruder, single-screw extrusion capable of a direct in-line feed of sc-CO_2 to the extruder barrel, and conventional twin-screw extrusion with PP-*g*-MA.

2. Experimental

2.1. Materials

Polypropylene (Pro-fax 6523, MFI = 4, density = 0.90 g/cm^3) was obtained from Basell (Elkton, MD) and was used as-received. Commercial RTP (Winona, MN) PP/PP-*g*-MA/clay nanocomposite sample prepared using a twin-screw extruder (TSE) was received in pellet forms. The clay concentration of the RTP sample determined from the burn-off method is 10 wt%. For the same level of comparison, it was diluted down to 4 wt% and 6.5 wt%. Surface modified montmorillonite (Cloisite 20A) was obtained from Southern Clay Products, Inc. (Gonzalez, TX) and was used as-is. Cloisite 20A is a surface modified montmorillonite obtained through a cation exchange reaction, where the sodium cation is replaced by dimethyl, dihydrogenated tallow, quaternary ammonium cation. Three other clays, namely Cloisite Na+, 93A, and 30B, were also considered. However, we chose to work with 20A because preliminary experiments using conventional single-screw extrusion technique in our laboratory showed that Cloisite 20A have better miscibility with PP and better property improvements than the other three [49]. Similar observations can also be found in other studies [50,51].

2.2. Clay concentration

Clay concentrations were determined by the burn-off technique in an ashing oven at 500 °C for 30 min. The reported concentrations are an average of three burn-off samples. The clay concentrations reported here include the intercalants or the organic modifiers.

2.3. Extrusion experiments

Polypropylene–clay nanocomposites were prepared by direct melt compounding and by using a modified pressurized chamber. Samples were extruded at a melt temperature of at around 190 °C and a screw speed of 15 rpm using a single, two-stage screw Killion KL-100 extruder with a 25.4 mm (1 in) diameter 30:1 *L/D*. A capillary die of 1/16 in diameter and 20:1 *L/D* was attached at the end of the extruder. The chamber is inserted between the CO_2 pump and the injection port at the beginning of the second stage of the screw. The overall system is shown schematically in Fig. 1. When using the pressurized chamber, the clays were allowed to be in direct contact with sc-CO_2 at 3000 psi and 80 °C for a period of time (12–24 h) and then the pressure was rapidly released. The mixture of the nanoparticles and sc-CO_2 was then injected into the molten polymer stream in a single-screw extruder. This is referred to as method #3.

In addition to the method just described, two other methods were used to prepare the nanocomposites.

Method #1 (direct melt blending): conventional single-screw melt compounding. The clay and PP were dry blended in a Kitchen Aid type mixer and then the mixture was fed to an extruder and re-pelletized.

Method #2: conventional single-screw melt compounding with in-line sc-CO_2 supply at the second stage of the screw. The clay and PP were dry mixed and fed to the extruder, as in method #1, but sc-CO_2 was added to the barrel during extrusion.

2.4. Injection molding

The nanocomposite pellets were dried at 100 °C in an oven overnight and then injection molded using an Arburg Allrounder Model 221-55-250 injection molder. The Arburg Allrounder has a 22 mm diameter barrel, $L/D = 24$, screw with variable root diameter from approximately 14.25 mm at the feed to 19.3 mm at the exit, a check ring non-return valve, and an insulated nozzle that is 2 mm in diameter. The composites were injection molded, using a melt temperature of 200 °C, a mold temperature of 80 °C, a holding pressure of 5 bar, and a screw speed of 200 rpm, and a rectangular end-gated mold with dimensions of 80 mm × 76 mm × 1.5 mm.

2.5. Dynamic mechanical thermal analysis (DMTA)

DMTA tests were done on injection molded plaques. Rectangular bars of dimensions 60 mm × 8.5 mm × 1.5 mm were cut from the plaques parallel to the flow direction. These bars were analyzed in the torsional mode of a Rheometrics Mechanical Spectrometer (RMS-800) at a strain of 0.2%, angular frequency of 1.0 rad/s, and heating rate of 5 °C/min. The dynamic temperature ramp was performed from 60 °C to 180 °C.

2.6. Rheological properties

Rheological studies of the nanocomposites were performed using a Rheometrics Mechanical Spectrometer Model 800 (RMS-800). Samples were prepared by compression molding the extruded pellets into 25 mm diameter disks. Dynamic frequency sweep experiments were performed under a continuous nitrogen atmosphere using a 25-mm parallel-plate fixture at 200 °C in the linear viscoelastic region of the materials. To determine the limits of linear viscoelastic properties of the materials, dynamic strain sweeps were performed at 200 °C and a frequency of 10 rad/s for a filled system with 6.7 wt% of 20A. From this result, it can be safe to perform dynamic frequency sweep experiments at a fixed strain of 5%, which is

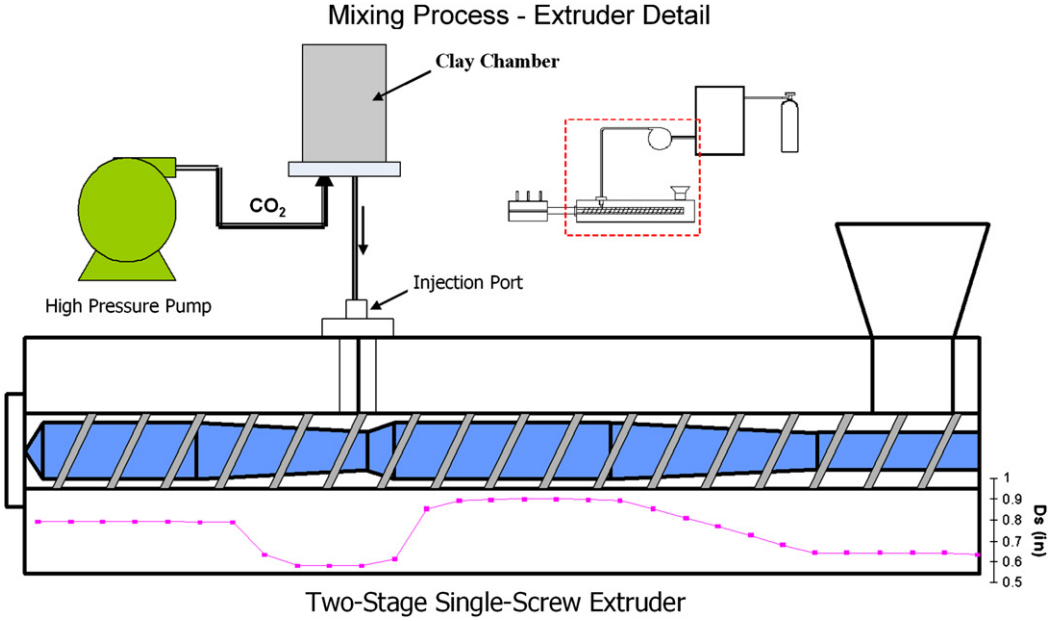

Fig. 1. Schematic diagram of the overall process showing the CO_2 chamber and the two-stage single-screw extruder.

well within the linear viscoelastic range of the materials investigated. The elastic moduli (G'), loss moduli (G''), and complex viscosities (η^*) of the materials as functions of angular frequency (ω) (ranging from 0.1 rad/s to 100 rad/s) are obtained.

2.7. Tensile properties

The injection molded plaques were cut into rectangular bars, typically along the machine direction, having dimensions of approximately 8.5 mm wide, 1.5 mm thickness, and 80 mm in length. Tensile tests on these bars were performed at room temperature using an Instron model 4204 testing machine. An extensiometer was used to accurately determine the elongation of the sample and hence Young's modulus and yield strength. The load was measured with a 5 kN load cell while the crosshead speed was kept at 1.27 mm/min during all tensile tests. For all tests, the average and the standard deviation were calculated from at least four samples, and data points greater than 2 standard deviations from the mean were omitted.

2.8. Structure and morphological characterization

The structure of the nanoclay and the morphology of the nanocomposites were analyzed by wide angle X-ray diffraction (WAXD) and transmission electron microscopy (TEM). WAXD patterns were conducted using a Scintag XDS 2000 diffractometer with Cu Kα radiation (wavelength = 1.542 Å) at a step size of 0.02° and a scan rate of 0.5°/min from 1.5° to 10°.

TEM micrographs were generated using a Philips EM420T with an accelerating voltage of 100 kV. The TEM samples, at around 95 nm thickness, were cut using a cryo-microtome equipped with a diamond knife at −100 °C.

3. Results and discussion

3.1. X-ray diffraction

WAXD patterns for pristine organoclay 20A, commercial RTP PP/PP-*g*-MA/clay nanocomposite, and PP/clay nanocomposites prepared via methods #1–3 are illustrated in Figs. 2 and 3, where Fig. 2 corresponds to WAXD patterns of extruded samples before injection molding and Fig. 3 represents WAXD patterns of injection molded samples. As shown in Fig. 2, the RTP extruded sample prepared via twin-screw extrusion with the incorporation of a compatibilizer shows a diffraction peak, which means that the nanocomposite is not fully exfoliated. This is a typical observation that is often seen in literature when dealing with PP–clay nanocomposites [31–42]. Similarly, the extruded sample prepared via method #2 also shows a diffraction peak, which suggests intercalated morphology. From the diffraction pattern, we can see that the peak is shifted to a lower angle compared to the pristine organoclay, which indicates some expansion of the clay gallery when exiting the extruder. This expansion could be due to both the CO_2 and the diffusion of polymer chains into the clay galleries. Comparing the diffraction patterns of the extruded samples prepared via methods #1 and #2, we see that the peak of sample prepared using method #2 is shifted not much lower than that of sample prepared using method #1, which leads us to believe that the expansion at the die due to CO_2 is not significant. On the other hand, WAXD patterns of extruded samples prepared via method #3 for 4 wt% and 6.6 wt% of 20A show no peaks, which may indicate fully exfoliated nanostructures. From this observation, we can conclude that the exfoliation of the layered silicate resulted from method #3 was not caused by the foaming of the CO_2 when exiting the extruder. Due to the limitation of the current technique, i.e. chamber design, we were not able to get exfoliated structure for clay concentration of 9.5 wt%. WAXD pattern for the nanocomposite at this concentration clearly indicates no expansion of the *d*-spacing. Therefore, no further analyses were done on concentrations higher than 6.6 wt%.

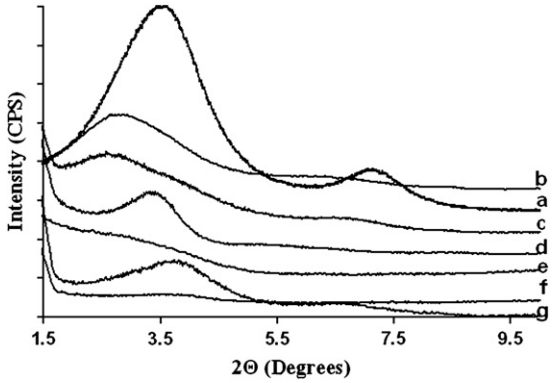

Fig. 2. WAXD patterns of extruded pellets before the injection molding step. (a) Cloisite 20A, (b) method #1: 4 wt%, (c) method #2: 4 wt%, (d) RTP TSE: 10 wt%, (e) method #3: 4 wt%, (f) method #3: 6.6 wt%, and (g) method #3: 9.5 wt%.

As the extruded product is melt processed further into other desired forms depending on the type of applications, the effect of additional processing on exfoliation must be examined. The nanocomposite structures upon subsequent melt processing, in this case injection molding, were examined by means of WAXD patterns which for various nanocomposites are shown

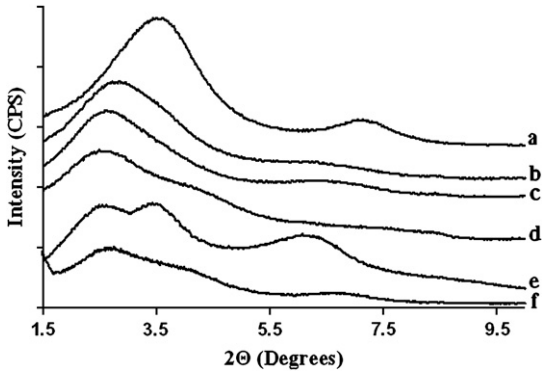

Fig. 3. WAXD patterns of different nanocomposites prepared using different methods. Tests were done on injection molded samples. (a) Cloisite 20A, (b) method #1: 4 wt%, (c) method #2: 4 wt%, (d) method #3: 4 wt%, (e) RTP TSE: 10 wt%, and (f) method #3: 6.6 wt%.

in Fig. 3. The resulting *d*-spacings determined from WAXD patterns are calculated from Bragg's law and are summarized in Table 1. We can see that commercial RTP sample and samples prepared via methods #1 and #2 all show peaks, but shifted to lower angles relative to pristine 20A, indicating expansion of the *d*-spacing due to intercalation of polymer between the galleries of the clay. The RTP sample shows a slight shift of the peak towards a lower angle, i.e. bigger *d*-spacing, compared to samples prepared via methods #1 and #2 due to the use of a compatibilizer and high shear processing. As observed in Fig. 2, WAXD patterns for the nanocomposite samples prepared using method #3 before the injection molding process show no peaks, but the peaks reappear after the injection molding process (Fig. 3), suggesting partial collapse and re-aggregation of the clay platelets during this process. This phenomenon was also observed by Alexandre et al. [52], who studied the thermodynamic stability of melt processed PE nanocomposites. The collapse observed here could suggest that the exfoliated nanocomposite structure is thermodynamically unfavorable for a highly non-polar polymer, such as PP, which has little to no attractive interactions with the clay itself. Looking at the WAXD pattern illustrated in Fig. 3 for the 4 wt% nanocomposite prepared via method #3, we see that the peak, however, is shifted to a lower angle, even lower than the ones shown by the RTP sample and samples prepared via methods #1 and #2, which indicates that the most expansion of the clay galleries still occurs in samples prepared by method #3. The WAXD patterns suggest that the method of using the pressurized CO_2 chamber is more effective in swelling and expanding, if not exfoliating, the clays and helps facilitate the intercalation of polymer into the clay galleries.

Although WAXD can offer a convenient method to determine the nanocomposite structure, not much can be concluded about the spatial distribution of the silicate layers. The nanocomposite structure, namely intercalated or exfoliated, may be identified by monitoring the position, shape, and intensity of the basal reflections from the distributed silicate layers. In fact, this has been studied by Kojima et al. [53] who used the peak intensity together with the peak position to characterize the relative proportion of exfoliated and intercalated species with the nanofiller content. However, peak broadening and intensity decreases are very difficult to study systematically, and thus, conclusions based solely on WAXD patterns are only tentative when concerning the mechanism of nanocomposite formation and their structure. To supplement the deficiencies of WAXD, TEM can be used. TEM allows a qualitative understanding of the internal structure, spatial distribution of the various phases, and views of the defect structure through direct visualization. TEM also has limitations. TEM is time consuming, and only gives qualitative information on a very small area, which may not entirely represent the microstructure of the nanocomposite as a whole. Regardless of their limitations, together, TEM and WAXD are essential tools for evaluating nanocomposite structure [54].

Table 1
d-Spacings for various nanocomposites calculated from Bragg's law

Sample description	2Θ (°)	d_{001} (Å)	% Increase
20A powder	3.58	24.66	–
Method #1: 4 wt%	2.86	30.87	25.17
Method #2: 4 wt%	2.64	33.44	35.60
RTP: 10 wt%	2.60	33.95	37.68
Method #3: 4 wt%	2.50	35.31	43.19
Method #3: 6.6 wt%	2.65	33.31	35.08

3.2. Transmission electron microscopy

To further confirm the degree of dispersion of the clay in the matrix, TEM analysis was carried out. TEM micrographs of various nanocomposites prepared using different processing techniques are presented in Figs 4–8. Two different magnifications at 17,000× and 34,000× are shown for each micrograph. As can be seen from Fig. 4, the 4 wt% nanocomposite prepared via method #1 represents an immiscible system with very large aggregates or tactoids in the order of several tens of silicate layers. Similarly, the extruded sample of the 4 wt% nanocomposite prepared using method #2 also contains many large tactoids (Fig. 5), which again proves that the foaming due to CO_2 at the die exit does not cause exfoliation of the clay platelets. TEM for the 4 wt% RTP sample

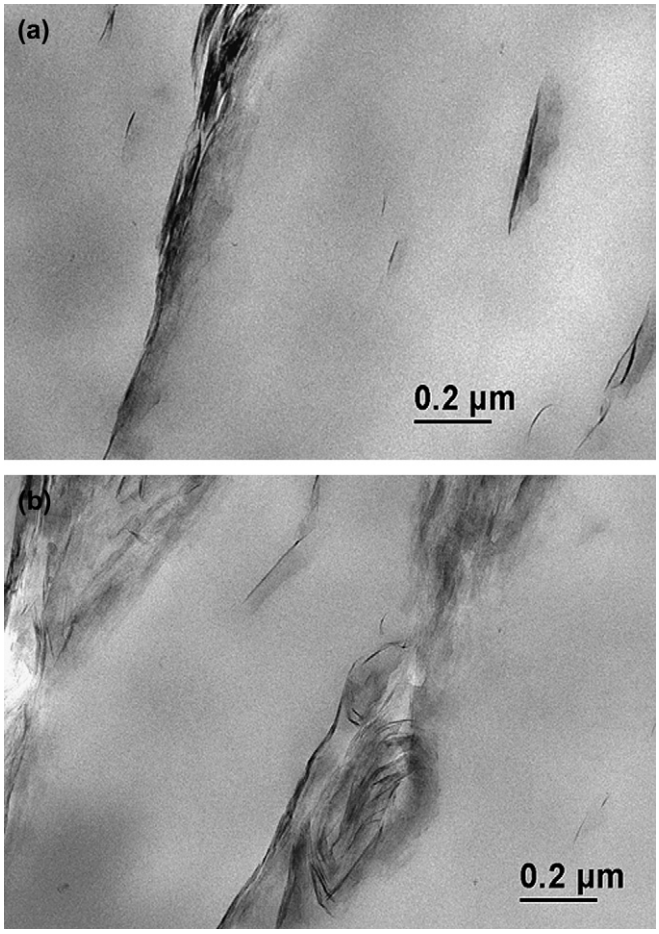

Fig. 4. Method #1: 4 wt% (a) 17,000× and (b) 34,000×.

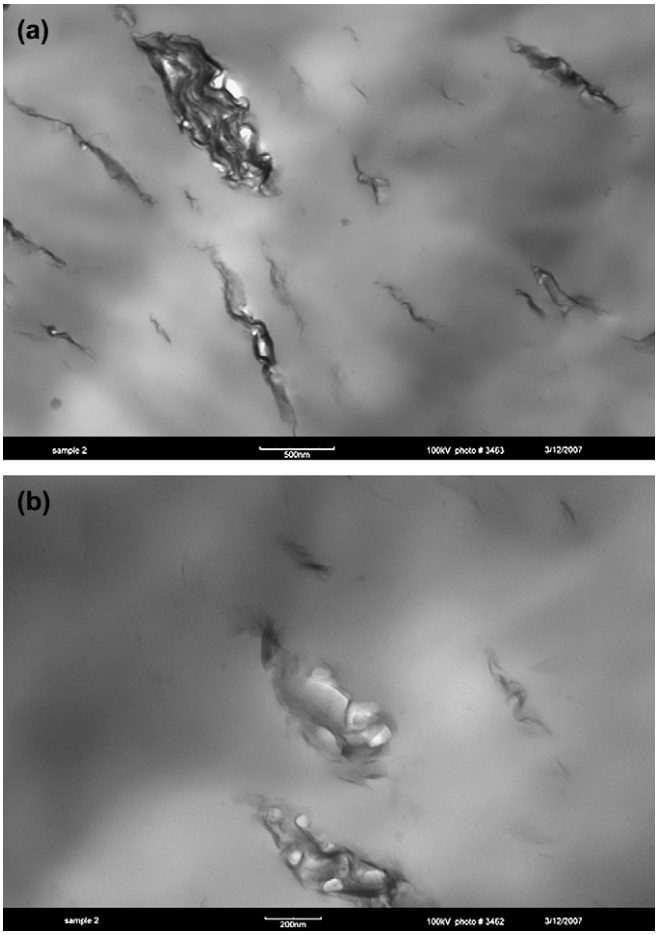

Fig. 5. Method #2: 4 wt% extruded pellets (a) 17,000× and (b) 34,000×.

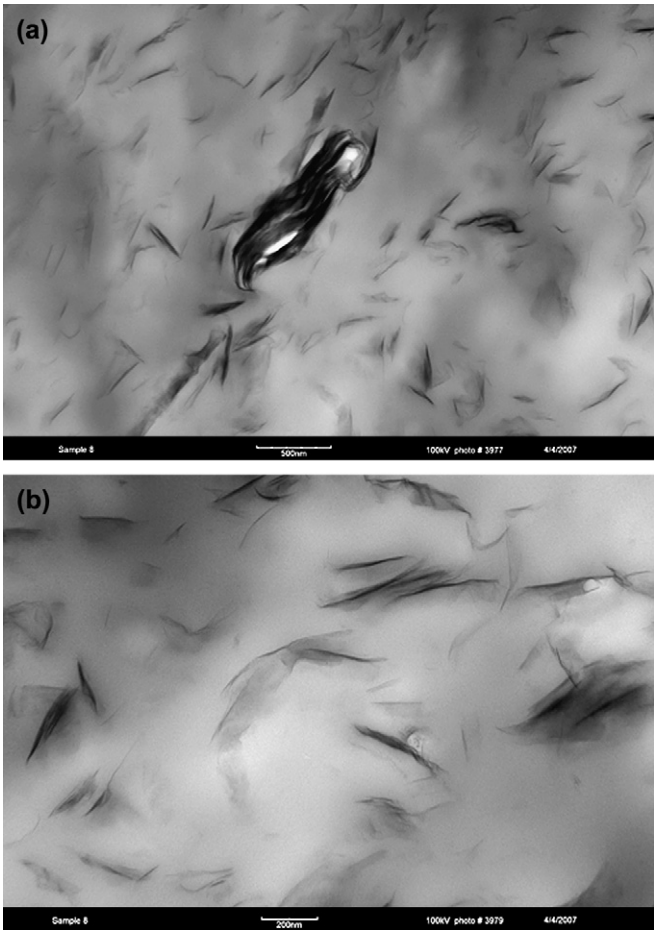

Fig. 6. RTP TSE: 4 wt% (a) 17,000× and (b) 34,000×.

is shown in Fig. 6. We can see better dispersion in the RTP nanocomposite compared to the other two methods due to the use of a twin-screw extrusion and an MAH compatibilizer. The best nanodispersion can be seen in the nanocomposites prepared using method #3 for concentration as high as 6.6 wt% clay (Figs. 7 and 8). Although, there are still some areas that show little aggregates, most show fairly well dispersed clay platelets even at high magnification. This observation is similar for the extruded sample and the injection molded sample. However, more little aggregates, but not as much as those observed in the other processing methods, were observed for the injection molded sample. This TEM observation confirms the WAXD patterns discussed in previous section.

3.3. Tensile properties

The tensile properties of various nanocomposites prepared via different processing techniques are summarized in Table 2 and Fig. 9. Pure polypropylene used in this study has a Young's modulus of 1.374 ± 0.133 GPa. With the addition of approximately 4 wt% Cloisite 20A, prepared via method #1, the nanocomposite was found to have a Young's modulus of 1.611 ± 0.059 GPa, an increase of about 17% compared to that of pure PP. Using the same technique, at concentration of 6.7 wt%, 10 wt%, and 14 wt% of 20A, the nanocomposites were found to have Young's moduli of 1.753 ± 0.045 GPa, 1.725 ± 0.130 GPa, and 1.787 ± 0.037 GPa, respectively. In other words, the modulus shows little increase beyond the addition of 4.0 wt% (when direct blended) which is a frequent observation [55–57]. It is important to note that using the direct melt-blending technique via single-screw extrusion, i.e. method #1, the properties leveled out at a clay level of 6.7 wt%. At clay concentration higher than 6.7 wt%, there was not much improvement in Young's modulus. This could be due to the formation of big agglomerates in the nanocomposite as shown by TEM. Aggregation of clay particles has been shown to reduce the amount of reinforcement that can be provided by the clays resulting in less enhancement of the Young's modulus [58]. For the nanocomposites prepared via method #2, moderate improvement in Young's moduli was observed when compared to those processed using method #1. This indicates a positive effect of the addition of sc-CO_2 during melt processing. For the RTP sample prepared via TSE with a compatibilizer, the highest Young's modulus was found to be at around 1.861 ± 0.068 GPa at 6.5 wt% of clay, an increase of about 35% compared to pure PP. Similar to the properties observed for samples prepared using methods #1 and #2, the properties for the RTP nanocomposite also

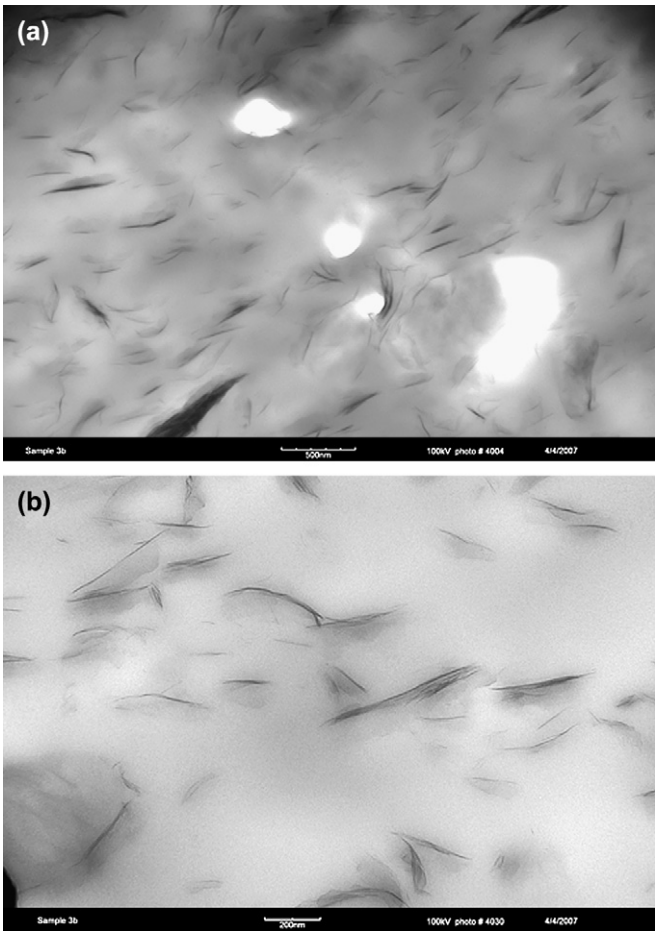

Fig. 7. Method #3: 6.6% extruded pellets (a) 17,000× and (b) 34,000×.

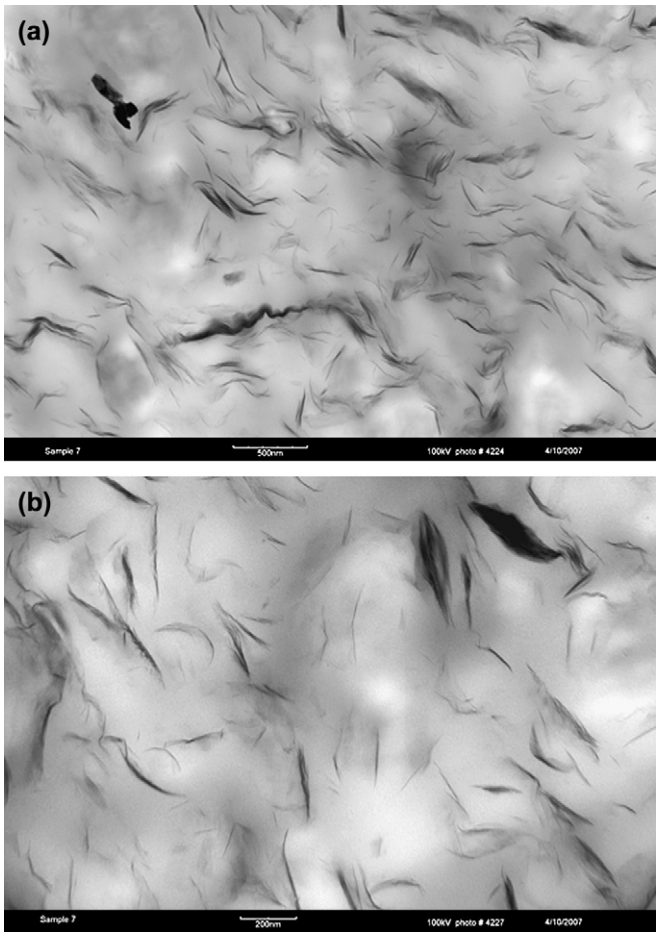

Fig. 8. Method #3: 6.6% injection molded sample (a) 17,000× and (b) 34,000×.

leveled off at around 6.5 wt% of clay. At the same level of clay concentration, the RTP nanocomposite possesses higher properties than those prepared via methods #1 and #2. This is due to the compatibilizer that was used in preparing the nanocomposite, which increased the bonding between the nanoparticles and the polymer matrix and, thus, helped better disperse clay in PP. Also, the RTP nanocomposite was prepared using a twin-screw extruder, which exerted high shear forces to break the clay platelets apart and helped to better mix and disperse the clays into the polymer matrix. The biggest improvement was seen when the nanocomposites were prepared using the pressurized CO_2 chamber. This agrees with the TEM and WAXD data that were discussed earlier. At 4 wt% of 20A, the nanocomposite was determined to have a Young's modulus of 1.848 ± 0.107 GPa, an increase of about 34% compared to pure PP, which is also a little higher than that of the RTP sample. At 4 wt% the nanocomposites prepared via method #3 possess slightly higher Young's modulus (1.848 GPa versus 1.769 GPa), higher yield strength (16.10 MPa versus 14.3 MPa), and higher elongation at break (80% versus 40%) than those of the RTP nanocomposite prepared using TSE with a compatibilizer. This means that method #3 can potentially replace the need for high shear processing and a compatibilizer and can still perform well in terms of tensile properties. At 6.6 wt%, an even bigger improvement in properties was observed. Young's modulus was increased to 2.118 ± 0.077 GPa, a 54% improvement compared to the base matrix. This indicates an essential contribution of the CO_2 chamber to the melt intercalation process in terms of expanding and exfoliating the nanoparticles into the polymer matrix. Also, the addition of sc-CO_2 during melt processing can enhance the mixing and the degree of intercalation/exfoliation of the clay into the polymer matrix. Although collapse and re-aggregation of the nanoparticles upon subsequent melt processing were observed, it is believed that the relative portion of the exfoliated structure remaining in the nanocomposites is still higher when the nanocomposite is prepared via method #3 than methods #1, #2, and TSE with PP-*g*-MA and hence, better improvements in tensile properties occur.

It is interesting to point out that the injection molded plaques of the nanocomposites processed using methods #1 and #2 appear to be opaque, whereas the ones prepared using method #3 appear to be a little shinier and more transparent. Presumably, higher degree of exfoliation of the clay into finer particles could be the reason why the sc-CO_2-treated samples appear more transparent than the non-treated samples. Nevertheless, the property enhancement observed here is not optimum, as will be shown by the composite theory, which is most probably ascribed to the combined effect of poor particle

Table 2
Tensile properties of various nanocomposites prepared using different processing methods

Materials	Young's modulus (GPa)	S.D.	% Increase	Yield strength (MPa)	S.D.	% Elongation	S.D.	HDT (°C)	S.D.
PP – pure	1.374	0.133	–	15.16	0.47	115.30	19.79	84.0	2.3
Method #1: 4 wt%	1.611	0.059	17	13.68	0.32	32.00	28.71	92.5	3.1
Method #1: 6.7 wt%	1.753	0.045	28	14.61	0.35	26.89	15.41	NA	NA
Method #1: 10 wt%	1.726	0.130	26	12.13	0.77	16.59	2.42	NA	NA
Method #1: 14 wt%	1.787	0.037	30	12.29	0.34	10.16	0.77	NA	NA
Method #2: 4 wt%	1.716	0.136	25	14.28	0.39	34.59	6.92	NA	NA
Method #2: 6.7 wt%	1.810	0.122	32	14.50	0.33	24.09	13.92	NA	NA
RTP TSE: 4 wt%	1.769	0.167	29	14.30	0.56	48.85	33.77	NA	NA
RTP TSE: 6.5 wt%	1.861	0.068	35	14.00	0.42	17.67	5.57	NA	NA
RTP TSE: 10 wt%	1.850	0.185	35	11.58	0.48	4.11	2.45	100.0	2.1
Method #3: 4 wt%	1.848	0.107	34	16.10	0.32	80.40	0.10	95.5	3.2
Method #3: 6.6 wt%	2.118	0.077	54	13.00	0.89	14.82	5.90	104.0	1.9

alignment in the test direction and the collapse of clay particles during the injection molding process. For optimum performance, the silicate must be fully exfoliated into individual layers and the platelets must orient parallel to the applied load direction.

In order to realize the full potential of mechanical property increase, it is necessary to compare the observed property enhancements, such as modulus, to those predicted by theories like those of Halpin–Tsai [34,59] and Ji et al. [64]. Realizing the full potential of mechanical property enhancement remains unclear even when fully exfoliated nanocomposite morphologies are shown by XRD. Evaluation of the expected modulus increase for polymer composites presented here will be based on two theories developed by Halpin–Tsai and Ji et al.

The effectiveness of the model to predict actual experimental values of Young's modulus depends on the assumptions it is based upon. Halpin and Tsai's model shown below in Eq. (1) assumes fully exfoliated clay platelets, unidirectional, i.e. well oriented filler particles, as well as a high degree of adhesion of the filler particles to the surrounding polymer matrix,

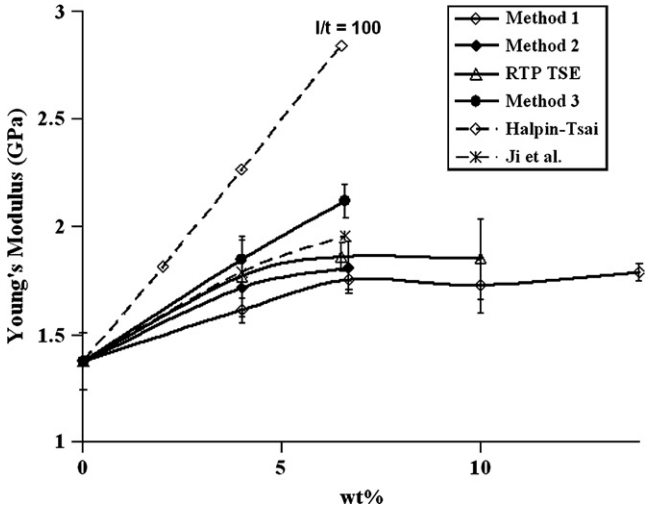

Fig. 9. Young's modulus of different nanocomposites versus clay weight percent as a function of different processing techniques.

$$E_c = E_m\left[\frac{1+\zeta\eta\phi_f}{1-\eta\phi_f}\right], \tag{1}$$

where E_c = composite modulus, E_m = unfilled matrix modulus, ϕ_f = filler volume fraction,

$$\eta = \frac{E_f/(E_m-1)}{E_f/(E_m+\zeta)}, \tag{2}$$

$$\zeta = 2(l/t), \tag{3}$$

E_f = filler modulus taken to be 178 GPa for MMT [34] and l/t = aspect ratio of the silicate platelets taken here to be approximately 100 for fully exfoliated platelets [34].

Contrary to the composite theory of Halpin and Tsai, the model developed by Ji et al. makes no assumption as to the state of clay orientation and so is valid for randomly oriented systems. Also, the model does not assume fully exfoliated clay particles. Ji et al.'s model takes into account three phases present in a polymer–clay nanocomposite, namely, the matrix, the filler, and the interphase region between the clay platelets with the polymer matrix residing within it. Ji's model can be described as follows,

$$\frac{1}{E_c} = \frac{1-\alpha}{E_m} + \frac{\alpha-\beta}{(1-\alpha)E_m + \alpha(k-1)E_m/\ln k} + \frac{\beta}{(1-\alpha)E_m + (\alpha-\beta)(k+1)E_m/2 + E_f\beta}, \tag{4}$$

where

$$\alpha = \sqrt{[2(\tau/t_c)+1]\phi_f}, \tag{5}$$

τ is the thickness of the interphase region taken to be the d-spacing, t_c is the thickness of MMT taken to be approximately 1 nm, $\beta = \sqrt{\phi_f}$, and $k = E_f/E_m$. Ji's model takes into account the interphase separation between clay particles and makes no assumption as to the state of intercalation or exfoliation of the clay platelets. If d-spacing data are available then the dependence of Young's modulus on the degree of intercalation can be determined.

The theoretical and experimentally measured moduli of the composites versus weight percent of MMT is shown in Fig. 9. As can be seen, the experimental Young's moduli presented are below those predicted by the Halpin–Tsai model. For the nanocomposites prepared using method #3, all values are about 20–30% lower than those predicted by the theory. For other methods, the difference is much bigger. This may be due to some important issues such as the lack of significant bonding between MMT and polypropylene because of the differences in the surface energies of hydrophilic MMT and hydrophobic PP, lack of complete orientation of the filler particles in the flow direction, and the aspect ratio may be less than the assumed value of 100.

Ji et al.'s model provides a closer prediction of Young's modulus because it is more valid for randomly oriented particles and it does not assume full exfoliation of the clay platelets. It was observed that the theoretically predicted modulus from Ji et al.'s model was within 3–10% of the experimentally obtained moduli for the nanocomposites, which is also close to the standard deviation. We noticed that Ji et al.'s model does not take into account the aspect ratio of the clay platelets nor the degree of dispersion of the particles within the polymer matrix. The *d*-spacing alone cannot tell how big the clay tactoids are or how well the particles are distributed. When the clay particles are more exfoliated and more dispersed it is expected that the values predicted by Ji's model should trail behind. This explains why Ji et al's theory underpredicts the values for the nanocomposites prepared via method #3.

3.4. Dynamic mechanical thermal analysis

Dynamic mechanical thermal analysis (DMTA) was performed on various nanocomposites to assess the effect of clay on the heat distortion temperature (HDT) as described by Scobbo [60]. The dynamic storage modulus of the nanocomposites versus temperature as a function of different processing methods is illustrated in Fig. 10. All the nanocomposites exhibit similar relative moduli curves versus temperature and possess a higher storage modulus than pure PP throughout the entire temperature range tested. The nanocomposite prepared via method #3 at 6.6 wt% of clay exhibits the greatest increase in the storage modulus. The vertical lines in Fig. 10 represent the HDT values for a stress of 0.45 MPa. The results are reported in Table 2. As can be seen, the heat distortion temperature increases with the addition of clay for all the nanocomposites. As much as 20° increase in the HDT at 6.6 wt% clay loading was observed for the nanocomposite prepared using method #3.

3.5. Rheology

In this section we look at the effect of the degree of exfoliation on the dynamic mechanical properties of melts containing various levels of nanoclay. In general it has been reported that when the nanoclays are exfoliated, a ''tail'' in the storage modulus, G', versus angular frequency is observed [61,62] at low frequencies. The tail is also reflected in the low frequency

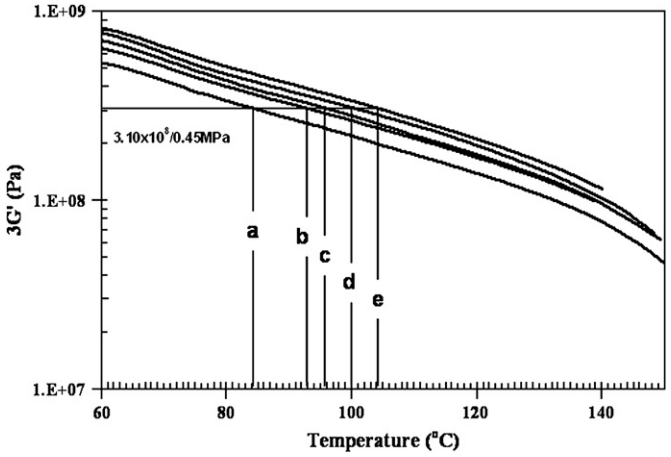

Fig. 10. $3G'$ as a function of temperature from DMTA. Vertical lines correspond to estimated HDTs. (a) PP, (b) method #1: 4 wt%, (c) method #3: 4 wt%, (d) RTP: 10 wt%, and (e) method #3: 6.6 wt%.

behavior of the magnitude of complex viscosity ($|\eta^*|$) as yield-like behavior. However, sufficient evidence for exfoliation is usually not supplied to confirm the degree of exfoliation.

The storage moduli, G', loss moduli, G'', and the complex viscosities, η^*, resulting from the dynamic frequency scan measurements are compared in Figs. 11–13, respectively. As can be seen in Fig. 11, big tactoids or agglomerates of clay can also exhibit the plateau or tailing effect at low frequencies as shown in Fig. 11. Larger aggregates can occlude and confine more polymer chains between the platelet layers. Thus, the increase of G', G'', and η^* might arise from the confinement of the polymer chains within the silicate layers. In fact, it has been shown that the viscosities of confined polymer melts are greater than those of bulk chains [63]. The RTP nanocomposite, which was confirmed by X-ray diffraction to be non-exfoliated, also shows a tail in G' at low frequencies. Also, the RTP nanocomposite possesses much higher values of G', G'', and η^* than the other nanocomposites prepared

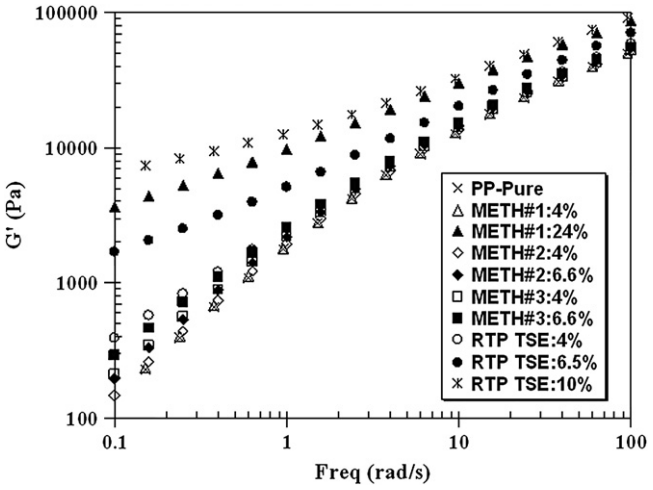

Fig. 11. Storage modulus versus frequency of different nanocomposites at 200 °C.

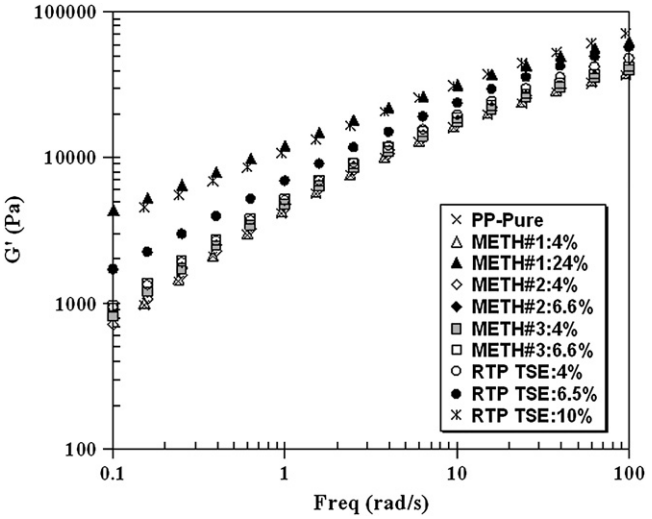

Fig. 12. Loss modulus versus frequency of different nanocomposites at 200 °C.

using the two described in this study. The reason for the increase of G', G'', and η^* could be attributed to the use of a maleic anhydride compatibilizer that increases interaction and hydrogen bonding between filler and polymer matrix, which probably leads to a lower polymeric chain mobility, making the material more rigid and solid-like. The nanocomposites synthesized by methods #1 and #3 do not show solid-like behavior at low frequencies and do not indicate the presence of a network structures. In fact, the two composites show process behavior similar to the neat unfilled PP resin. The extruded sample, prepared by method #3, as shown by XRD and TEM data contains nanoclay that appears to be fairly exfoliated and dispersed, shows no tail in the G'. Here, the lack of a tail in the G' could be due to the absence of a network formed by the strong hydrogen bonding between the polar functional group of PP-*g*-MAH group and the oxygen group of the silicate. In addition, the confinement effect is largely reduced due to a fairly dispersed structure of the silicate.

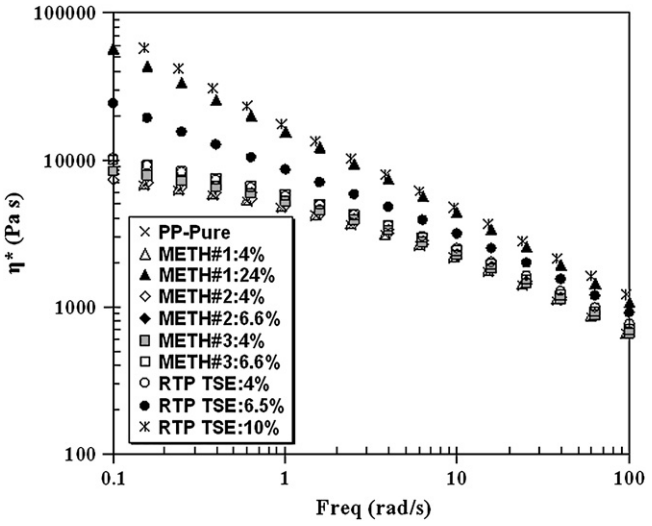

Fig. 13. Complex viscosity versus frequency of different nanocomposites at 200 °C.

Therefore, regardless of the fine dispersion of the clay tactoids, the increase in G', G'', and η^*, is less pronounced for the nanocomposites prepared using method #3.

Using rheology to determine the degree of exfoliation of the nanocomposites is still ambiguous. Therefore, conclusions regarding the morphology based on the rheological data presented here cannot be made. What can be concluded from this rheological study is the processability of the nanocomposites. The shear viscosities of the nanocomposites prepared via method #3 (Fig. 13) are much lower than that of RTP sample prepared using TSE. Therefore, it can be concluded that PCNs prepared via method #3 should have better processability than the ones synthesized by TSE with a compatibilizer.

4. Conclusion

In this work, an environmentally benign process was developed to help exfoliate and disperse nanoclay into the polymer matrices at high clay content. Evidence from WAXD, TEM data, and improvements of the material properties, such as Young's modulus, yield strength, and HDT, lead us to believe that the technique of using the pressurized CO_2 chamber has significant potential as a benign and efficient process for exfoliating and dispersing nanoclays into polymer melts. By allowing the clay to be in direct contact with sc-CO_2, expanding via quick pressure release, and injecting the mixture into the polymer melt, great improvement in the exfoliation of the clay into the polymer matrix was observed. In the supercritical state, CO_2 behaves as a polar organic solvent. It is hypothesized that CO_2 readily enters the galleries of the nanoclay (treated with alkyl quaternary ammonium salts) and swells the alkyl chains. When the pressure is partially released, CO_2 expands the galleries and, thereby, further exfoliates the clay particles. Furthermore, CO_2 is partially soluble in a number of polymers and further facilitates the mixing process. With the aid of sc-CO_2, more exfoliated clay particles were achieved. The presence of exfoliated clay greatly enhanced the mechanical and rheological properties of the nanocomposites. As observed, the conventional direct melt compounding methods, with and without the direct injection of CO_2, did not show much improvement in the mechanical properties due to their inability to adequately exfoliate the nanoparticles into the polymer matrix. The commercial RTP sample prepared using a TSE and an MAH compatibilizer showed moderate improvements over methods #1 and #2. However, most improvements were seen from the technique of using the pressurized CO_2 chamber. WAXD and TEM data showed a good degree of exfoliation for concentrations as high as 6.6 wt% and mechanical properties such as modulus increased by as much as 54%.

Acknowledgements

This work was supported by the Environmental Protection Agency (grant #: R-82955501-0) and the National Science Foundation (grant #: CTS-0507995). We express gratitude to the VPI&SU Materials Science & Engineering colleagues for their aid in conducting the XRD studies.

References

[1] Usuki A, Kojima Y, Kawasumi M, Okada A, Fukushima Y, Kurauchi T, et al. J Mater Res 1993;8:1185.
[2] Kojima Y, Usuki A, Kawasumi M, Okada A, Kurauchi T, Kamigaito O. J Polym Sci Part A Polym Chem 1993;31:983.
[3] Kojima Y, Usuki A, Kawasumi M, Okada A, Kurauchi T, Kamigaito O. J Polym Sci Part A Polym Chem 1993;31:1755.
[4] Liu L, Qi Z, Zhu X. J Appl Polym Sci 1999;71:1133.
[5] Lan T, Kaviratna D, Pinnavaia J. Chem Mater 1994;6:573.
[6] Gilman W, Morgan A, Giannelis P, Wuthenow M, Manias E. Flame retardancy 10th annual BBC conference proceedings; 1999. p. 1.
[7] Giannelis P. Appl Organomet Chem 1998;12:675.
[8] Okada A, Kawasumi M, Usuki A, Kojima Y, Kurauchi T, Kamigaito O. In: Schaefer W, Mark E, editors. Polymer based molecular composites. MRS symposium proceedings, vol. 171. Pittsburgh; 1990. p. 45–50.
[9] Giannelis P. Adv Mater 1996;8:29.
[10] Giannelis EP, Krishnamoorti R, Manias E. Adv Polym Sci 1999;138:107.
[11] LeBaron PC, Wang Z, Pinnavaia TJ. Appl Clay Sci 1999;15:11.
[12] Vaia RA, Price G, Ruth PN, Nguyen HT, Lichtenhan J. Appl Clay Sci 1999;15:67.
[13] Biswas M, Sinha S. Adv Polym Sci 2001;155:167.
[14] Gilman JW. Appl Clay Sci 1999;15:31.
[15] Bins & Associates. Plast Addit Compd 2002;4(1):30–3.
[16] Sall K. Eur Plast News March 14, 2002.
[17] Messersmith PB, Giannelis EP. J Polym Sci Part A Polym Chem 1995;33:1047.
[18] Gilman JW, Kashiwagi T, Lichtenhan JD. SAMPE J 1997;33:40.
[19] Dabrowski F, Bras L, Bourbigot S, Gilman JW, Kashiwagi T. Proceedings of the Eurofillers, vol. 6. France: Lyon-Villeurbanne; 1999. p. 9.
[20] Bourbigot S, LeBras M, Dabrowski F, Gilman JW, Kashiwagi T. Fire Mater 2000;24:201.
[21] Gilman JW, Jackson CL, Morgan AB, Harris R, Manias E, Giannelis EP, et al. Chem Mater 2000;12:1866.
[22] Blumstein A. J Polym Sci Part A Polym Chem 1965;3:2665.
[23] Theng BKG. Formation and properties of clay–polymer complexes. Amsterdam: Elsevier; 1979.
[24] Krishnamoorti R, Vaia A, Giannelis P. Chem Mater 1996;8:1728.
[25] Kawasami M, Hasegawa N, Kato M, Usuki A, Okada A. Macromolecules 1997;30:6333–8.
[26] Nam PH, Maiti P, Okamoto M, Kotaka T, Hasegawa N, Usuki A. Polymer 2001;42:9633–40.
[27] Kato M, Usuki A, Okada A. J Appl Polym Sci 1997;66:1781–5.
[28] Modesti M, Lorenzetti A, Bon D, Besco S. Polymer 2005;46:10237–45.
[29] Kanny K, Moodley VK. J Eng Mater Technol 2007;129:105–12.
[30] Lee JW, Kim MH, Choi WM, Park OO. J Appl Polym Sci 2006;99:1752–9.
[31] Alexandre M, Dubois P. Mater Sci Eng 2000;28:1.
[32] Ray SS, Okamoto M. Prog Polym Sci 2003;28:1539.
[33] Pinnavaia TJ, Beall GW. Polymer–clay nanocomposites. New York: J Wiley & Sons; 2000.
[34] Fornes TD, Paul DR. Polymer 2003;44:4993.
[35] Osman MA, Rupp JEP, Suter UW. Polymer 2005;46:1653.
[36] Wang ZM, Nakajima H, Manias E, Chung TC. Macromolecules 2003;36:8919.
[37] Manias E. Origins of the materials properties enhancements in polymer/clay nanocomposites. In: Golovoy A, editor. Nanocomposites 2001, delivering new value to plastics. Chicago: ECM Inc.; 2001.
[38] Koo CM, Kim JH, Wang KH, Chung IJ. J Polym Sci Part B Polym Phys 2005;43:158–67.
[39] Dennis HR, Hunter DL, Chang D, Kim S, White JL, Cho JW, et al. Polymer 2001;42:9513.
[40] Manias E, Touny A, Wu L, Strawhecker K, Lu B, Chung TC. Chem Mater 2001;13:3516.
[41] Svoboda P, Zeng CC, Wang H, Lee LJ, Tomasko DL. J Appl Polym Sci 2002;85:1562.
[42] Ellis TS, D'Angelo JS. J Appl Polym Sci 2003;90:1639.
[43] Garcia-Leiner M, Lesser AJ. ANTEC 2004;1528:32.
[44] Zerda AS, Caskey TC, Lesser AJ. Macromolecules 2003;36:1603.
[45] Caskey TC, Lesser AJ. Polym Eng Sci 2001;84:134.
[46] Wingert MJ, Han Z, Zeng C, Li H. ANTEC 2003;986:990.
[47] Mielewski DF, Lee EC, Manke CW, Gulari E. US Patent 6,753,360; 2004.
[48] Manke CW, Gulari E, Mielewski DF, Lee EC. US Patent 6,469,073; 2002.
[49] Nguyen QT, Baird DG. Process for increasing the exfoliation and dispersion of nanoclay particles into polymer matrices using supercritical carbon dioxide, Ph.D. dissertation. Virginia Polytechnic Institute and State University; 2007.
[50] Lopez-Quintanilla ML, Sanchez-Valdes S, Ramos de Valle LF, Medellin-Rodriguez FJ. J Appl Polym Sci 2006;100:4748–56.
[51] Zhu L, Xanthos M. J Appl Polym Sci 2004;93:1891–9.
[52] Alexandre M, Dubois P, Sun T, Garces JM, Jerome R. Polymer 2002;43:2123.
[53] Kojima Y, Usuki A, Kawasumi M, Okada A, Kurauchi T, Kamigaito O. J Polym Sci Polym Chem Ed 2001;39:1360.
[54] Morgan AB, Gilman JW. J Appl Polym Sci 2003;83:1329–38.
[55] Hasegawa N, Okamoto H, Kawasumi M, Kato M, Tsukigase A, Usuki A. Macromol Mater Eng 2000;280:76.
[56] Reichert P, Nitz H, Klinke S, Brandsch R, Thomann R, Mülhaupt R. Macromol Mater Eng 2000;275:8.
[57] Kim KN, Kim H, Lee JW. Polym Eng Sci 2001;41:1963.
[58] Fornes TD, Yoon PJ, Keskkula H, Paul DR. Polymer 2001;42:9929.
[59] Halpin JC, Kardos JL. Polym Eng Sci 1976;16:344.
[60] Scobbo Jr JJ. Thermomechanical performance of polymer blends. In: Paul DR, Bucknall CB, editors. Polymer blends. Performance, vol. 2. New York: Wiley; 2000. p. 335.
[61] Litchfield DW, Baird DG. The rheology of high aspect ratio nano-particle filled liquids. Rheol Rev 2006;1–60.
[62] Wagener R, Reisinger TLG. Polymer 2003;44:7513.
[63] Leungo G, Schmitt FJ, Hill R, Israelachvili J. Macromolecules 1997;30:2482.
[64] Ji XL, Jing JK, Jiang W, Jiang BZ. Polym Eng Sci 2002;42:983.